Coherent Interfaces between Crystals in Nanocrystal Composites

Hongwei Liu,[†] Zhanfeng Zheng,[†] Dongjiang Yang,[†] Xuebin Ke,[†] Esa Jaatinen,[†] Jin-Cai Zhao,[‡] and Huai Yong Zhu[†,*]

[†]Chemistry, Queensland University of Technology, QLD 4001, Australia, and [‡]Institute of Chemistry, The Chinese Academy of Science, Beijing 100080, China

ABSTRACT Numerous materials are polycrystalline or consist with crystals of different phases. However, materials consisting of crystals on the nanometer scale (nanocrystals) are not simply aggregates of randomly oriented crystals as is generally regarded. We found, that in four different materials that consist of nanocrystals of two different phases and were obtained by different approaches, the nanocrystals of different phases are combined coherently forming interfaces with a close crystallographic registry between adjacent crystals (coherent interfaces). The four materials were fabricated by (i) depositing Ag_2O nanoparticles on titanate nanofibers, (ii) phase transition from TiO_2(B) nanofibers to the nanofibers of mixed TiO_2(B) and anatase phases, (iii) dehydration of the single crystal fibril titanate core coated with anatase nanocrystals, and (iv) attaching zeolite Y nanocrystals on the surface of titanate nanofibers. The finding suggests that preferred orientations and coherent interfaces generally exist in nanocrystal systems, and according to our results, they are largely unaffected by the fabrication process that was used. This is because the preferred orientations require that the engaged crystal planes from two connected crystals have the same basal spacing and that the crystals can interlock tightly at the atomic level to form thermodynamically stable interfaces. Hence it is rational that the preferred orientations and coherent interfaces dominant the nanostructures formed between the different nanocrystals and play a key role in assembling the composite nanostructures. The orientation and interfaces between crystals of different phases in mixed-phase materials are extremely difficult to determine. Nonetheless, the thermodynamic stability of the coherent interfaces allows us to apply phase-transformation invariant line strain theory to predict the preferred orientation (and thus the structure of the coherent interfaces). The theoretical predications agree remarkably with the transmission electron microscopy (TEM) analysis. This implies that we may acquire knowledge of the orientation and the interface structures in the mixed-phase materials without TEM measurement, and the knowledge is essential for comprehensively understanding properties of the many materials and processes that depend on the interfaces.

KEYWORDS: interface · nanocrystal · assembly · transmission electron microscopy

The interfaces between crystals of different phases (crystal interfaces or interphase boundaries) play an important role in determining the structure of materials that consist of nanocrystals[1−3] because of the large relative fraction of atoms that exist in the interfacial regions.[4] These crystal interfaces are important as many properties of the solid materials formed depend on them. For example, a random connection of two different crystals would lead to dangling bonds, large crystallographic discrepancies, and voids in the interface region. These structural imperfections can significantly affect many of the physical and chemical properties of the materials. Conversely, if two different nanocrystals join at surfaces of crystallographic similarity, then the formation of chemical bonds between atoms of opposing surfaces is maximized and full coordination can be achieved. Bonding between two phases reduces overall energy by minimizing surface energy associated with unsatisfied bonds. Such coherence between two nanocrystals results in a reduction of Coulomb forces and a minimization of dangling bonds, thereby creating stable interfaces. The interfaces between nanocrystals, formed by phase transformation, reaction, or spontaneous attachment are different from those formed by other forces, such as magnetic and electron static forces, confining or jamming forces, capillary forces, and friction and lubrication forces. The latter plays an important role in assembling nanoparticles and has been extensively studied,[5] while the former is much less understood at the atomic level because the crystallographic features of interfaces are very difficult to investigate, although nanocrystals are assembled by these interfaces in many advanced materials. It has been reported recently that the interfacial orbitals undergo "reconstruction" when oxide crystals combined coherently.[6,7] This is an important finding for understanding the behavior of high-temperature superconductors and ferromagnets of oxides that have a perovskite structure with similar lattice parameters, as it ensures well-matched interfaces. The crystal interfaces are determined by the relative orientation between the adjacent crystals. Particles consisting of two mixed phases have been generally regarded as aggregates of randomly

*Address correspondence to hy.zhu@qut.edu.au.

Received for review July 20, 2010 and accepted August 31, 2010.

Published online September 7, 2010. 10.1021/nn101708q

© 2010 American Chemical Society

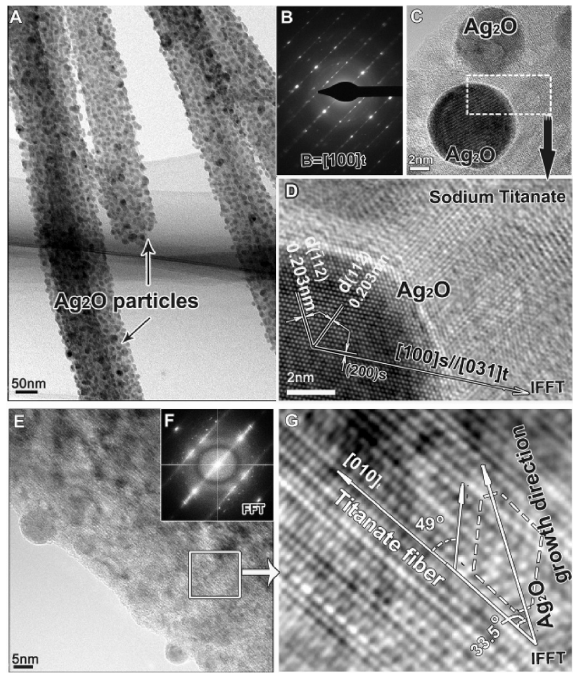

Figure 1. (A) TEM analysis of the Ag_2O nanoparticles deposited on the sodium titanate surface. A large number of Ag_2O nanoparticles with size <10 nm are observed homogenously distributed on the titanate fiber surface. (B) The surface has a planar normal $[100]_t$, confirmed by selected electron diffraction pattern. (C) An image of a spherical Ag_2O particle is shown. (D) Image was obtained by inversing the FFT of the image in C. The lattice fringes in this image can be observed clearly. It can be seen in D that the orientation of $[100]_s$ is parallel to $[031]_t$.

oriented crystals, and thus there should be an infinite array of crystal interfaces with no statistically dominant interface structure prevailing throughout the material. But this hypothesis may not be valid in many nanocrystalline materials, since preferential oriented attachment of nanoparticles has been observed in self-assemblies of nanocrystals.[8−11] Therefore, this raises the question: is the phenomenon that two nanocrystals combine coherently forming interfaces with a close crystallographic registry (*i.e.*, coherent interface) a typical feature that exists across a diversity of nanocrystal systems, or does it simply arise in a few specific systems and situations? If it is a predominant feature, then determining what the principle underlying this phenomenon is and understanding it well enough to be able to predict the coherence between the constituent nanocrystals becomes important.

Answers to these questions would lead to two important outcomes. First, the structure of the coherent interfaces and thus the orientation may be predicted from knowledge of the interface energy and the lattice parameters of the crystals involved. Second, if an oriented attachment is a common phenomenon in many systems of nanocrystals, then it would therefore play an important role in the assembly and self-assembly of these crystals in advanced material fabrication.

While it is readily accepted, the hypothesis that particles of two different phases are aggregates of randomly oriented crystals has never been verified for nanocrystalline materials. Unlike aggregates of large particulate materials, in nanocrystal systems, the constituent nanoparticles have a relatively large surface area to volume ratio, and thus the surface energy accounts for a considerable fraction of the overall system energy. An argument can then be said that when a large fraction of atoms exist in the interface regions, such as in nanocrystal aggregates, the thermodynamic stability of the coherent interfaces with a close crystallographic registry dominates the overall stability of the system. Hence, coherent interfaces and thus the orientation between nanocrystals should widely exist in nanostructural materials. Unfortunately, the structural information revealing the orientation of nanocrystals and the nature of the interfaces can be extremely difficult to determine even with high-resolution transmission electron microscopy (HRTEM). This lack of knowledge is a serious impediment to developing a comprehensive understanding of the properties of polycrystal materials and in designing new functional materials based on nanocrystals.

In this study, we determine the structure of the coherent interfaces between crystals of two different phases in four systems (and thus the crystallographic orientation of the crystals of one phase to the crystals of another phase) by using transmission electron microscopy (TEM) and predict it by applying phase-transformation invariant line strain (ILS) theory. The four systems are: (1) Ag_2O nanoparticles depositing on the titanate nanofibers, (2) the nanofibers of mixed TiO_2(B) and anatase phases obtained from nanofibers of TiO_2(B) by phase transition, [TiO_2(B) is a polymorph of titanium oxide with monoclinic baddeleyite-like form; here "B" represents baddeleyite as the lattice of this TiO_2 polymorph and is very similar with baddeleyite (a rare zirconium oxide mineral)], (3) the nanofibers of a single crystal TiO_2(B) coated with anatase nanocrystals obtained from the nanofibers of mixed anatase and titanate phases, which involves a dehydration reaction ($H_2Ti_3O_7$ to TiO_2), and (4) zeolite Y nanocrystals attached on the surface of titanate nanofibers. The choice of nanofibers for this investigation was important as the nanofiber morphology is particularly well suited for TEM study of the crystal interface structure, in contrast to irregular shaped or spherical particles with mixed phases. The fibers have thicknesses of several tens of nanometers, and TEM micrographs can provide clear information about the lattice structures of fibers with such dimensions. Also, the directions of the engaged lattices relative to the fibril axis can be ascertained because the fibers always lay flat on the specimen holder making it simpler to determine the relative orientation of the lattices.

RESULTS AND DISCUSSION

Ag_2O Nanocrystal-Bonded Na-Titanate Nanofibers. Figure 1 shows the TEM images of Ag_2O particles deposited on the surface of Na-titanate nanofibers. Titanate nanofiber was identified by electron diffraction pattern shown in Figure 1B. Ag_2O (PDF card number 43-0997) has a crystal structure with space group $pn\bar{3}m$ and lattice parameter $a = 0.4726$ nm. TEM and HRTEM investigations have confirmed that the Ag_2O nanoparticle size does not exceed 15 nm (see single particle shown in Figure 1C and D, an inverse fast flourier transformation (IFFT) image of 1C) and that they are homogenously and densely distributed on the titanate surface as shown in Figure 1A and E. There exists a closed crystallographic registry between the Ag_2O and Na-titanate phase, as we have found that all of Ag_2O articles have the same crystallographic registry with respect to the substrate fibers. In Figure 1E is shown an HRTEM image of Ag_2O particles distributed on titanate fibers. Figure 1F and G are the fast Fourier transform (FFT) and IFFT images corresponding to Figure 1E. That is, the direction $[02\bar{1}]_s$ is parallel to $[100]_t$, and the plane $(112)_s$ is parallel to $(013)_t$. The subscripts "t" and "s" are for titanate and silver oxide, respectively. The crystallographic orientation relationship (COR) can be expressed in low index as $(\bar{1}10)_s//(\bar{1}\bar{1}\bar{1})_t$, $[111]_s//[011]_t$, and $[11\bar{2}]_s//[110]_t$. (See Figure 1G and detailed calculation in Section S1 of the Supporting Information.)

The best matching of a crystal with an adjacent crystal is achieved when the interface between the two crystals has a minimum misfit strain, and the system of two crystals has minimal interfacial energy, resulting in coherent interfaces and in the creation of the most stable structure. Thus we can apply the ILS theory to determine the structure under which the minimum interface strain occurs.[13] According to ILS theory, the crystallographic orientation relationship between the initial phase and a newly formed phase in many diffusion-controlled phase transitions can be derived by matching the lattices of the two phases and rotating one lattice relative to the other.[13−16] If the difference between the two crystals at the interface, for example, the interplanar spacing (d-space) of the two crystals, is large, rotating one lattice about a principal axis (*e.g.*, "*Z*" axis) will be necessary to minimize the interface strain. Such a rotation can be calculated using eq 1, which was derived using matrix algebra:[17]

$$\cos\theta = \frac{1 + \eta_1\eta_2}{\eta_1 + \eta_2} \tag{1}$$

Here θ is the angle of lattice rotation, and η_1 and η_2 are the principal distortions required to make the two lattices coincident. Best matching of one crystal with the other is achieved when the interface between them has a minimum misfit strain and the system of the two crystals has low interfacial energy. To match the lattices of two crystals, multiple rotation operations may be required, and the details of the operations are given in a previous work.[18]

Obviously, once the interfaces with minimum interface strain are determined, the orientations between the crystals of different phases are also known. In process (1), silver oxide nanocrystals formed on the Na-titanate surface can be treated as an epitaxial growth. The invariant line theory can be applied for epitaxial growth by considering the habit plane at the surface of the substrate. Ag_2O has a cubic structure, and Na-titanate has a monoclinic structure ($C2/m$, $a = 0.8570$, $b = 0.3800$, $c = 0.9135$ nm, $\beta = 101.57°$). There is a simple lattice correspondence relationship between the cubic phase and monoclinic phase, that is, $[101]_t$ corresponds to $[100]_s$, $[010]_t$ to $[010]_s$, and $[\bar{1}01]_t$ to $[001]_s$. Set the main strains for the three axes as η_1, η_2, and η_3 and the habit plane denoted as $(hkl)_t$, whose normal is parallel to $[100]_t$. By resolving the following equations:

$$\begin{cases} x^2 + y^2 + z^2 = 1 \\ \dfrac{x^2}{\eta_1^2} + \dfrac{y^2}{\eta_2^2} + \dfrac{z^2}{\eta_3^2} = 1 \\ hx + ky + lz = 0 \end{cases} \tag{2}$$

An invariant line or growing direction $[x, y, z]_s$ was found to be $[0.3276, 0.8380, \overline{0.4347}]_s$ after considering coordinate transition. This direction has a departure angle of 33° from $[010]_t$. The COR between the two phases was also derived theoretically to be close to observed OR and is provided in Section S1 of the Supporting Information.

The results demonstrate that coherent interfaces exist in system (1), the heterogeneous epitaxy of Ag_2O nanocrystals deposited on the Na-titanate nanofibers, and the orientation of the Ag_2O nanocrystals with respect to the Na-titanate fibers can be successfully derived using crystallographic theory. Supported Ag_2O nanoparticles have been found to be active catalysts in selective catalytic reduction of NO_x.[19] To prevent losing the Ag_2O nanoparticles in the catalytic operation, the nanoparticles have to be well bonded to the support. The Ag_2O-coated titanate nanofibers prepared in this study will be competitive as Ag_2O nanoparticle catalysts in such applications, since they are strongly and stably bonded to the fibers through the formation of coherent interfaces. Oxygen atoms at the interfaces are shared by the two phases.

Phase Transition from TiO_2(B) Nanofibers to the Nanofibers of Mixed TiO_2(B) and Anatase Phases. TEM and HRTEM analysis indicates the fibril morphology was maintained during the phase transition under heating (Figure S1 in the Supporting Information), and in the product, TiO_2(B) and anatase phases coexisted in a single nanofiber. The electron diffraction patterns of the mixed phase nanofibers are shown in Figure S2A−D of the Supporting In-

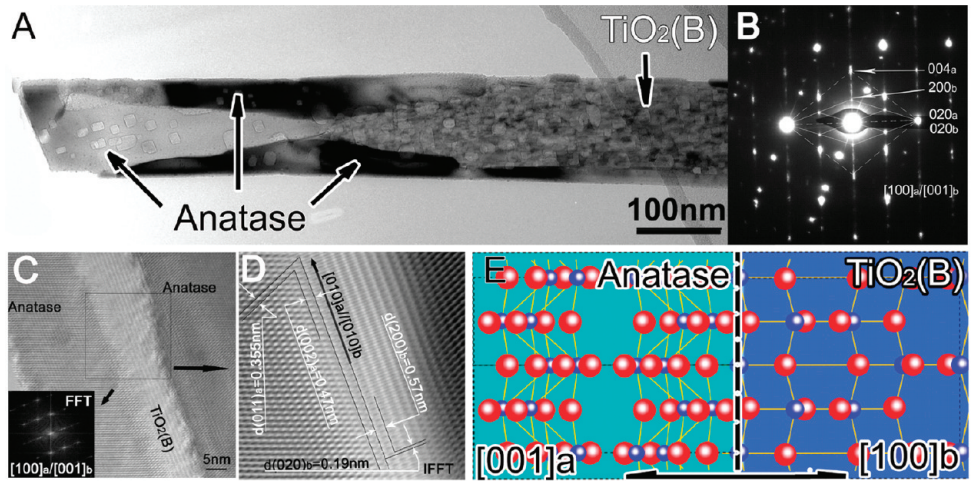

Figure 2. Microstructure and interface structure of a T600 nanofiber with mixed TiO_2(B) and anatase phases. (A) TEM micrograph of a T600 nanofiber, which was obtained by calcining TiO_2(B) at 600 °C. Anatase phase is adjacent with the residual TiO_2(B) phase, and the fibril morphology was maintained during the phase transition under heating. (B) Composite electron diffraction patterns of the sample T600 taken down $[100]_a$ and $[001]_b$. (C) HRTEM image of the interface between anatase and TiO_2(B) phases, and the inset is a FFT image corresponding to the square area marked with a dash line. (D) Inverse FFT image from the square area in C, illustrating the good matching between plane $(002)_a$ and plane $(200)_b$. The crystallographic orientation relationship (COR-1) between the two phases could be expressed as $[100]_a//[001]_b$ and $(001)_a//(100)_b$. (E) Atomic arrangement down $[100]_a$ and $[001]_b$ of the interface formed by connection of $(010)_a$ and $(010)_b$ planes in the fibers of mixed anatase and TiO_2(B) obtained from process (2).

formation. T600 fiber, calcined at 600 °C and consisted of mixed TiO_2(B) and anatase, was chosen as a representative to study the interface structure and crystallographic orientation relationship between the two phases. According to the TEM analysis, the crystallographic orientation relationship between the two phases can be expressed as $[100]_a//[001]_b$ and $(001)_a//(100)_b$ and from here on will be referred to as COR-1. The symbol "//" indicates that the two items are parallel, and the subscripts "a" and "b" are for anatase and TiO_2(B), respectively. The orientation relationship in this system, expressed by composite stereographic projections of plane and direction, are shown in Figure S3A and B of the Supporting Information. The stereographic projection of the crystal plane is different than that of the crystal direction, even though they have the equivalent pole center, if the crystal structure is not cubic. Both of them are shown to make the crystallographic orientation relationship between anatase and TiO_2(B) better to understand. Indeed, there are preferred crystallographic orientations of anatase crystals with respect to TiO_2(B) crystals in the mixed-phase fibers. In these nanofibers, the interface is formed by connecting the $(010)_a$ plane in anatase with the $(010)_b$ plane of TiO_2(B) crystals. The $(010)_a$ planes of anatase have a basal spacing of 0.378 nm, close to that of the $(010)_b$ planes (0.374 nm) in the adjacent TiO_2(B) (Figure 2C and D, its IFFT image). With $(001)_a$ parallel to $(100)_b$, the structure has an appearance that $(001)_a$ and $(100)_b$ have the same orientation so that the (010) plane of anatase extends across into the adjacent phase TiO_2(B) (see Figure 2E). It also follows that since the number of pairs of parallel planes, which have similar basal spacing, is finite and that the number of the types of interfaces between the two phases is limited. Banfield and coworkers[20] have also discovered that in polycrystalline rutile the single crystals attach to one other with a preferred orientation. In this study, the two phases were also identified by HRTEM and electron diffraction. For comparison, the TEM images of pure TiO_2(B) fibers, the mixed-phase fibers obtained at different calcining temperatures, and the pure anatase fibers are provided in Figure S1 of the Supporting Information.

ILS theory was also applied for predicting the crystallographic orientation relationship between two TiO_2(B) and anatase crystals in the nanofibers obtained from process (2). We found that the crystallographic features, including the orientation relationship and interface predicted by the theory, agreed well with those obtained experimentally from TEM measurements. The detailed procedures and results are given in Section S3 of the Supporting Information.

Dehydration of the Single Crystal Fibril Titanate Core Coated with Anatase Nanocrystals. In system (3), the anatase thin plates formed first on the surface of the H-titanate nanofibers have a relatively regular polygonal morphology (see Figure 3A). The interface structure and crystallographic registry between the two phases were also determined. It shows that $[100]_a$ is nearly parallel to $[001]_t$ and that there is a slight divergence (about 2°) between plane $(011)_a$ and $(110)_t$, as shown in the stereographic projection (see Figure S3 in the Supporting Information).

After calcinations at 450 °C, the H-titanate core converted into a TiO_2(B) single crystal, while anatase nanocrystals remained on the surface of the TiO_2(B) fiber (see Figure 4A). The interface structure and crystallographic registry between the anatase thin plates and the TiO_2(B)

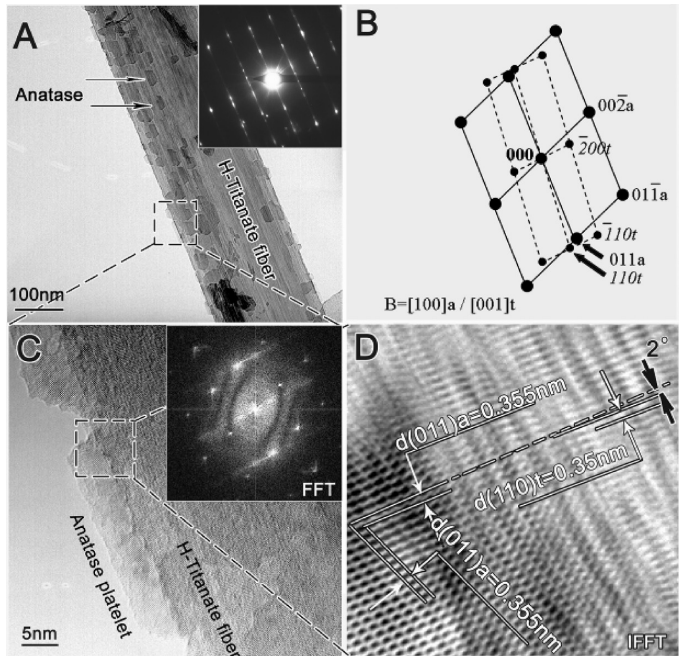

Figure 3. Microstructure of H-titanate fibers covered with anatase platelets. (A) TEM image of such a fiber with an in-set showing the corresponding electron diffraction patterns. The anatase thin plates on the surface of the H-titanate nanofibers have a relatively regular polygonal morphology. (B) Index of the FFT image in C, the incident beam direction is $B = [100]_a/[001]_t$. (C) HRTEM image of an anatase particle on the surface of H-titanate fiber, and the in-set is an FFT image showing the electron diffraction patterns of the involved phases anatase and H-titanate. (D) Inverse FFT image from the square area in C. It indicates that plane $(011)_a$ is nearly parallel to plane $(110)_t$. As summarized in B, $[100]_a$ is nearly parallel to $[001]_t$, and there is a slight diverge (about 2°) between plane $(011)_a$ and $(110)_t$.

nanofiber core were also investigated and shown in Figure 4D, F, and G. An inverse fast Fourier transform image (Figure 4F) was obtained from the pattern shown in Figure 4E. Figure 4C and F clearly indicate that the plane $(011)_a$ in anatase is parallel to plane $(110)_b$ in TiO_2(B) and that both of them have the same interplanar spacing. The crystal interface between the two phases is $(110)_b//(011)_a$. The resulting crystallographic orientation relationship, referred to as COR-2, in these core/shell structure fibers can be summarized by the following planar and directional relationships: $(011)_a//(110)_b$, $[100]_a//[001]_b$, and $[010]_a$ is nearly parallel to

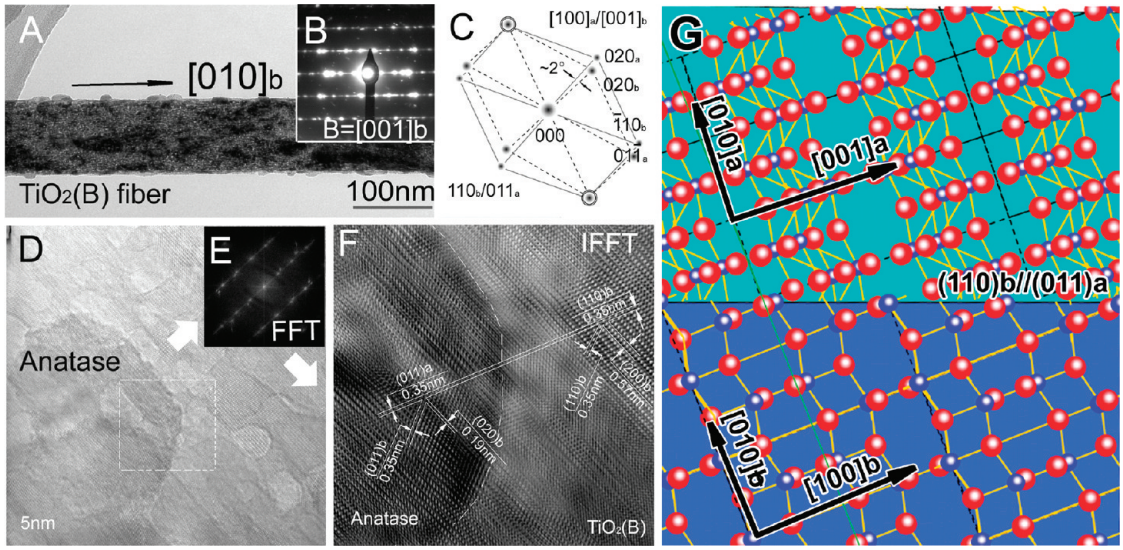

Figure 4. Microstructure of TiO_2(B) fibers covered by anatase platelets. (A) TEM micrograph of single TiO_2(B) fiber. (B, inset) Corresponding electron diffraction patterns taken down in $B = [001]_b$. (C) Index of the FFT image (E). (D) HRTEM image of an anatase particle on the surface of a TiO_2(B) fiber. (E) FFT image giving the matching pattern between anatase and TiO_2(B). (F) Inverse FFT image from the marked area in D, indicating a good match between plane $(011)_a$ and $(110)_b$. The resulting crystallographic orientation relationship (COR) in the fibers obtained from process (3) (COR-2) can be summarized by the following directional relationships: $(011)_a//(110)_b$, $[100]_a//[001]_b$, and $[010]_a \sim /[010]_b$, with a divergence of about 2° from the experimental observations as shown in C. (G) Atomic arrangement in the interface region illustrates the interface structure of the fibers of TiO_2(B) coated with anatase nanocrystals, obtained from process (3).

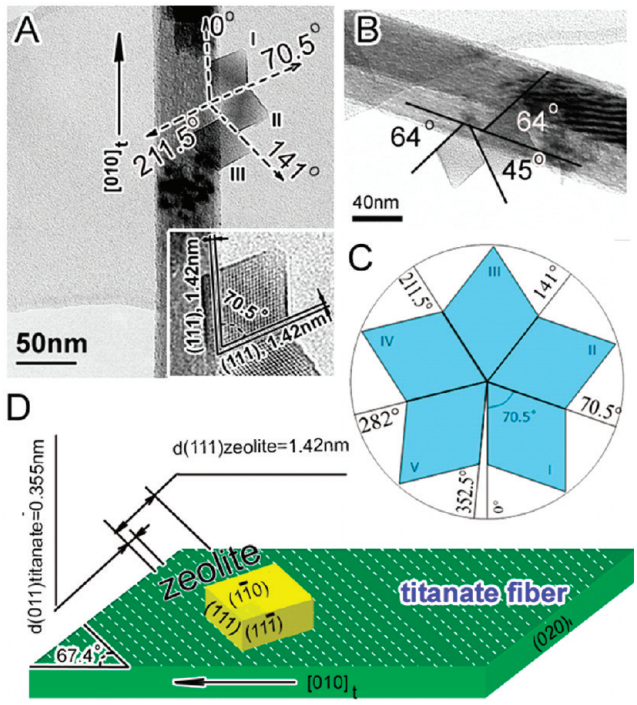

Figure 5. Preferred orientations in the assembly of titanate coated with zeolite Y nanocrystals. (A) and (B) TEM images showing the induced angles between zeolite (111) plane and titanate (001) plane parallel to $[010]_t$. (A, inset) Enlarged lattice fringes of the zeolite particle and the interplane distance of (111) planes. (C) Possible self-assembly of zeolite Y nanoparticle of rhombic shape and enclosed by {111} and {110} planes. Here the symbol {} means that the planes involved belong to a crystal plane family, *e.g.*, {111} includes eight planes (111), (11$\bar{1}$), (1$\bar{1}$1), ($\bar{1}$11), ($\bar{1}\bar{1}$1), ($\bar{1}$1$\bar{1}$), (1$\bar{1}\bar{1}$) and ($\bar{1}\bar{1}\bar{1}$). A maximum of five zeolite crystals can connect each other at a planar surface by forming coherent interfaces with their (111) planes. This allows six possible departure angles between every two (111) planes as listed in Table S3 of the Supporting Information. (D) 3-D profile of the zeolite nanocrystals attaching on the surface of titanate nanofiber by keeping their (111) plane parallel to the (011) plane of the fiber. Please note that the interplane distance of $(111)_z$ is 1.42 nm, exactly four times of that of $(011)_t$ (0.355 nm).

$[010]_b$ with a small divergence of about 2°, as determined from the experimental observations (Figure S3B and E of the Supporting Information). A schematic profile of such an interface is shown in Figure 4G, illustrating the atomic arrangement in the interface region. It demonstrates that the crystallographic orientation relationship between the anatase and the TiO_2(B) phase in the fiber has the $(011)_a$ plane parallel to $(110)_b$, with the $[100]_a$ direction parallel to $[001]_b$. This indicates that the orientation of the anatase crystals with respect to the TiO_2(B) crystals in the fibers obtained from process (3) is the same as that observed in the mixed-phase fibers of system (2).

The above conclusion is also confirmed by the theoretical ILS analysis of System (3). To match the lattices of TiO_2(B) and anatase (lattice correspondence), we set the body diagonal line of the tetragonal anatase phase, $[111]_a$, parallel to the face diagonal line of monoclinic TiO_2(B) phase $[110]_b$.[21] The predicted crystallographic features, including the crystallographic orientation relationship, invariant line, and crystal interfaces, are listed in Tables S1 and S2 of the Supporting Information. The detailed calculation procedure is also given in Sections S3 and S4 of the Supporting Information. The new crystallographic orientation relationship derived by applying the ILS theory is in good agreement with that observed in the TEM analysis, and the conclusion that new crystallographic orientation relationship in the core/shell structure nanofibers is the same as COR-1 observed in process (2) is also illustrated by the stereographic projection of orientation and plane (Figure S3A and B of the Supporting Information).

These results reveal that in mixed-phase fibers the anatase crystals always connect with TiO_2(B) crystals in preferred orientations regardless of the fabrication process. Intrinsically this is because the preferred orientation between the crystals results in a thermodynamically stable structure when the interface strain is at a minimum. This is also the reason that the choice of fabrication process had only a minor influence on the orientation and the interface structure. Actually, it is an implied prerequisite for the application of the ILS theory that the preferred orientations and the coherent interface structures of the mixed phase systems are independent of the fabrication process. The above results offer strong support that ILS theory can be successfully used to predict the crystallographic orientation relationship between different crystals obtained *via* various fabrication processes.

It should be noted that more than one type of crystal interface can exist for a particular crystallographic orientation relationship between TiO_2(B) and anatase crystals. For example, other possible interfaces in the nanofibers of system (2) are revealed in the stereographic projection of the plane displayed in Figure S3B of the Supporting Information. Some of the possible interfaces include $(10\bar{3})_a$//$(302)_b$ formed by connecting the $(10\bar{3})_a$ plane of anatase with the $(302)_b$ plane of TiO_2(B) crystals, $(010)_a$//$(010)_b$ and $(001)_a$//$(100)_b$. However, it is difficult to observe all of the possible interface structures with HRTEM.

Zeolite Y Nanocrystals Attached on the Surface of H-Titanate Nanofibers. System (4) is more complicated in which zeolite Y nanocrystals were attached on the surface of the titante nanofibers *via* two types of coherent interfaces: the coherent interfaces between zeolite and titanate and between zeolite Y nanocrystals (a self-assembly of zeolite nanocrystals). Images of zeolite Y nanocrystals attached on the surface of the titanate fiber are shown in Figure 5A and B.

The nanocrystals of zeolite Y have a rhombic morphology enclosed by planes {110} and {111} (see Figure 5D). Planes (020) and (011) are often observed in the [100] direction for titantate nanofibers (see Figure 5D). At first glance of the TEM images, it appears no clear dominant orientation of the zeolite crystals exists with respect to the substrate fibers, as the zeolite crystals could attach to the fibers in various orientations. How-

TABLE 1. Comparison of Crystallographic Features between the Predictions of the ILS Theory with the Results of TEM Analysis for All the Four Systems

systems	comparing features	theoretic values(deg)	measured values(deg)	δ(°)
titanate/Ag_2O[a]	orientation relationship	$(\bar{1}10)_s 3.5^\circ \rightarrow (\bar{1}1\bar{1})_t$; $[111]_s 4.4^\circ \rightarrow [011]_t$; $[11\bar{2}]_a 4.7^\circ \rightarrow [110]_t$	$(\bar{1}10)_s // (\bar{1}1\bar{1})_t$; $[111]_s // [011]_t$; $[11\bar{2}]_a // [110]_t$	<4.8
TiO_2(B)/anatase[b]	orientation relationship	$(001)_a // (100)_b$; $[100]_a 0.5^\circ \rightarrow [001]_b$; $[010]_a 0.5^\circ \rightarrow [010]_b$	$(001)_a // (100)_b$; $[100]_a // [001]_b$; $[010]_a // [010]_b$	0.5
TiO_2(B) core/anatase shell[c]	orientation relationship	$(011)_a // (110)_b$; $[100]_a 1.6^\circ \rightarrow [001]_b$; $[010]_a 1.6^\circ \rightarrow [010]_b$	$(011)_a // (110)_b$; $[100]_a 2.0^\circ \rightarrow [001]_b$; $[010]_a 2.0^\circ \rightarrow [010]_b$	0.4
Titanate/zeolite Y[d]	planar matching	67.4	64; 70.5	3.4; 3.1
		42.1	45	2.9
		29.4	28.6; 33	1.8; 2.9
		18.6	20.2	1.6
		49.9	49	0.9

[a]Orientation relationship calculated has a small departure (smaller than 5°) against the experimental observation. [b]$[010]_a$ is nearly parallel to $[010]_b$ with a divergence of 0.5°, and so is $[100]_a$ to $[001]_b$. [c]$[010]_a$ is nearly parallel to $[010]_b$ with a divergence of 2.0° and so is $[100]_a$ to $[001]_b$. [d]Induced angle between the trace of plane $(111)_z$ and $[010]_t$, the long axis of titanate fiber regarding to six variants.

ever, given that the *d* value of the plane (111) of zeolite Y (1.42 nm) is four times that of the *d* value of the plane (011) of the titanate fibers (0.355 nm), it is expected that the (111) plane of zeolite should preferentially align itself parallel to the (011) plane of titanate to achieve the best matching with the titanate fibers. The orientation of the zeolite crystals relative to the nanofibers can be determined from the TEM analysis (such as Figure 5A and B and the selected area electron diffraction). The first zeolite particle is attached on titanate in an orientation where the (111) plane of zeolite is parallel to the (011) plane of titanate (an assembly process, schematically shown in Figure 5D). Other zeolite particles will then connect to particle 1 with their (111) planes aligned [(111) plane to (111) plane, a self-assembly process]. There should be five orientations for the self-assembled zeolite Y crystals on a planar surface. This is because the internal angle between (111) planes is 70.5° for a cubic structure. As a result, all zeolite particles exhibit six orientations with respect to the substrate titanate nanofiber. As shown in Figure 5C, the six possible orientations of the zeolite crystals expressed as the angle between plane $(111)_z$ and $(011)_t$ are 0°, 70.5°, 142°, 211.5°, 282°, and 352.5°, respectively. The theoretically predicted possible orientations and those experimentally observed by TEM are listed in Table 1. Crystallographic features between the predictions of the ILS theory with the results of TEM analysis for all the four systems, as well as in Table S3 and Figure S6 of the Supporting Information, which show that all observed orientations agree with the predicted orientations with a discrepancy that is less than 3.5°, are also summarized in Table 1.

Assemblies of zeolite nanocrystals on titanate nanofibers discussed here are of great practical importance.[22,23] The coherent interfaces in the system prevent zeolite nanocrystals from being lost in catalytic operation, greatly improving yield of products. Also we could control aggregation of the nanocrystals as well as the pore entrances to be exposed by adjusting the population of the zeolite crystals on the fiber and by utilizing the defined orientation of the zeolite nanocrystals to the substrate, as shown in Figure S6 of the Supporting Information. This can significantly improve the accessibility of the active sites of the zeolite nanocrystals and enhance adsorption selectivity and catalytic performance of zeolite Y.

The results presented here for the materials of systems (1) and (4) are of significance not only for research of catalysts, where zeolite nanocrystals and noble metal oxide nanoparticles play important roles, but also for understanding the assembling processes that occur in nanocrystal systems when other functional structures and devices are fabricated from nanocrystals. The component crystal phases in these systems are chemically different substances and are not related by phase transitions. The system described by process (4) is more complicated, involving two assembling mechanisms: assembling zeolite Y crystals with titanate and self-assembling zeolite Y nanocrystals. Assembling various nanocrystals by different mechanisms in one system also has great potential for producing new unique functional structures.

The results obtained by HRTEM and ILS analyses for the four systems are compared in Table 1, which indi-

cates that we are able to predict the structure of nanocrystal assemblies by applying the ILS theory.

Finally it is also important to note that all the coherent interfaces studied in the present work are formed under thermodynamic control. Many nanostructure fabrications are under kinetic control, and the interfaces between nanocrystals formed in these processes may be different from those in this study. An example is the heteroepitaxial interfaces between different crystals of a nanocomposite prepared from solution (under kinetic control) changed when the sample was annealing at high temperatures (under thermodynamic equilibrium conditions).[24] The interfaces formed in kinetic control processes are worth future investigation.

CONCLUSIONS

Both high-resolution transmission electron microscopy (HRTEM) and invariant line strain (ILS) analysis confirms that the preferred orientation between nanocrystals of different phases exists in all four systems discussed here. Since the preferred orientations between crystals of different phases can result in thermodynamically stable coherent interfaces, we are able to predict the structure of nanocrystal assemblies by applying ILS theory. The results obtained by HRTEM and ILS analyses for the four systems well support this conclusion. The fabrication process has little influence on the preferred orientation. We infer that preferred orientations and formation of coherent interfaces are expected to exist widely in systems of nanocrystals. Once the crystallographic orientation relationship between two phases involved is known, the atomic arrangements of the coherent interfaces, as shown in Figures 2E and 4G, can be derived with crystallographic knowledge of the phases. This will allow us to know the orientation and interface structures in many solids of nanocrystal composites by applying ILS theory, without needing to experimentally determine the overall structure by conducting HRTEM measurements that are often difficult to perform. The knowledge acquired in this study is essential for understanding the properties of nanostructural materials, including nanocrystal self-assembly, and the relative orientation of the crystals in nanocrystal composites.

METHODS

In this study, four systems were investigated to determine how two nanocrystals of different phases combine coherently by forming interfaces with a close crystallographic registry between adjacent crystals.

System (1). Sodium titanate ($Na_2Ti_3O_7$, or Na-titanate) nanofibers were employed as support to coat silver oxide (Ag_2O) nanocrystals. For instance, 200 mg Na-titanate nanofibers, which were synthesized by a reaction between concentrated NaOH solution and a titanium compound under hydrothermal conditions (200 °C),[12] were dispersed into 200 mL pure water. The pH value of the suspension was adjusted to ~11 by adding diluted sodium hydroxyl aqueous solution dropwise. The nanofibers were collected by centrifuging and were added into 200 mL 1×10^{-2} M silver nitrate aqueous solution. After stirring for 24 h, the solid was collected and dried at 80 °C for 12 h.

System (2). Nanofibers of mixed TiO_2(B) and anatase (TiO_2) phases were obtained from nanofibers of TiO_2(B) by phase transition. The TiO_2 nanofibers were prepared from the protonated titanate ($H_2Ti_3O_7$, or H-titanate) nanofibers that were obtained by treating Na-titanate nanofibers with dilute HCl acid solution.[12] Heating H-titanate nanofibers at temperatures between 550 and 700 °C results in nanofibers of mixed TiO_2(B) and in anatase phases because of gradual phase transition, while calcinations at a temperature of 700 °C or above yields pure anatase fibers. The calcination temperature is indicated in the sample name: for instance, samples T300 and T400 were the samples calcined at 300 and 400 °C, respectively.

System (3). Nanofibers of a single crystal TiO_2(B) coated with anatase nanocrystals were obtained from H-titanate ($H_2Ti_3O_7$) nanofibers.[12] The H-titanate nanofibers were dispersed in a dilute (0.05M) HNO_3 acid solution and kept at a designed temperature for 2 days. The external surface of H-titanate nanofibers was converted into anatase nanocrystals of 10−20 nm in size, while the fiber core remained in the titanate phase. Subsequent heating at 450 °C converted the H-titanate core of the acid-treated fibers into TiO_2(B) by a dehydration reaction ($H_2Ti_3O_7$ to TiO_2). We obtained composite nanofibers with a TiO_2(B) core coated with anatase nanocrystals.

System (4). Zeolite Y nanocrystals were attached on the surface of $H_2Ti_3O_7$ nanofibers. The surface charges of the H-titanate fibers were first modified using poly(diallydimethylammonium chloride) surfactant, and then the fibers were coated with zeolite Y seeds in an alkali solution. The zeolite Y seeds were prepared with molar composition of $1Al_2O_3$:$4.35SiO_2$:2.4TMAOH:1.2TMABr:$0.048Na_2O$:249 H_2O. The loaded zeolite seeds further grew to nanocrystals by consuming a zeolite precursor solution with a similar composition (with higher water content). The fibers loaded with zeolite seed were dispersed in the precursor solution. The size and distribution of the zeolite crystals on the fibers were controlled by tuning the experimental conditions of growth process and the quantity of the loaded zeolite seeds.

The structures of the composite nanofibers of the four systems were investigated by transmission electron microscopy (TEM) using a Tecnai F20 microscope operating at 200 kV. The specimens for TEM studies were prepared by dispersing and depositing a drop of the sonicated ethanol suspension samples onto a copper grid coated with a holey carbon film.

Acknowledgment. Financial Supports from the Australian Research Council (ARC DP0877108), the National Science Foundation of China (nos.20537010 and 20777076), and the 973 project (2007CB613306) are gratefully acknowledged.

Supporting Information Available: The details of crystallographic investigations on titanate nanofibers grown with Ag_2O particles in process (1), nanofibers of mixed TiO_2(B) and anatase phases in process (2), procedures for predicting the COR in the nanofibers obtained from processes (2) and (3), and crystallographic orientation relationship between zeolite Y and titanate in process (4). This material is available free of charge *via* the Internet at http://pubs.acs.org.

REFERENCES AND NOTES

1. Tsukazaki, A.; Ohtomo, A.; Kita, T.; Ohno, Y.; Ohno, H.; Kawasaki, M. Quantum Hall-effect in Polar Oxide Heterostructures. *Science* **2007**, *315*, 1388–1391.
2. Reyren, N.; Thiel, S.; Caviglia, A. D.; Kourkoutis, L. F.; Hammer, G.; Richter, C.; Schneider, C. W.; Kopp, T.; Rüetschi, A. S.; Jaccard, D.; et al. Superconducting Interfaces between Insulating Oxides. *Science* **2007**, *317*, 1196–1199.
3. Chakhalian, J.; Freeland, J. W.; Habermeier, H.-U.; Cristiani,

G.; Khaliullin, G.; van. Veenendaal, M.; Keimer, B. Orbital Reconstruction and Covalent Bonding at an Oxide Interface. *Science* **2007**, *318*, 1114–1117.
4. Lu, K.; Lu, L.; Suresh, S. Strengthening Materials by Engineering Coherent Internal Boundaries at the Nanoscale. *Science* **2009**, *324*, 349–352.
5. Min, Y. J.; Akbulut, M.; Kristiansen, K.; Golan, Y.; Israelachvili, J. The Role of Interparticle and External Forces in Nanoparticle Assembly. *Nat. Mater.* **2008**, *7*, 527–538.
6. Först, C. J.; Ashman, C. R.; Schwarz, K.; Böchl, P. E. The Interface between Silicon and a High-k Oxide. *Nature* **2003**, *427*, 53–56.
7. Dagotto, E. When Oxides Meet Face to Face. *Science* **2007**, *318*, 1076–1077.
8. Pacholski, C.; Kornowski, A.; Weller, H. Self-assembly of ZnO: from Nanodots to Nanorods. *Angew. Chem., Int. Ed.* **2002**, *41*, 1188–1191.
9. Korgel, B. A.; Fitzmaurice, D. Self-assembly of Silver Nanocrystals into Two-dimensional Nanowire Arrays. *Adv. Mater.* **1998**, *10*, 661–665.
10. Whitesides, G. M.; Grzybowski, B. Self-assembly at all Scales. *Science* **2002**, *295*, 2418–2421.
11. Huang, F.; Zhang, H. Z.; Banfield, J. F. Two-stage Crystal-growth Kinetics Observed during Hydrothermal Coarsening of Nanocrystal-line ZnS. *Nano Lett.* **2003**, *3*, 373–378.
12. Zhu, H. Y.; Lan, Y.; Gao, X. P.; Ringer, S. P.; Zheng, Z. F.; Song, D. Y.; Zhao, J. C. Phase Transition between Nanostructures of Titanate and Titanium Dioxides via Simple Wet-chemical Reactions. *J. Am. Chem. Soc.* **2005**, *127*, 6730–6736.
13. Dhamen, U. Orientation Relationships in Precipitation Systems. *Acta Metall.* **1982**, *30*, 63–73.
14. Luo, C. P.; Dahmen, U. Interface Structure of Facet Lath-shaped Cr Precipitate in a Cu-0.33%wtCr Alloy. *Acta Metall.* **1998**, *46*, 2063–2081.
15. Luo, C. P.; Weatherly, G. C. The Precipitation Behaviour of a Zr-2 5 wt %Nb Alloy. *Metall. Trans.* **1988**, *19A*, 1153–1160.
16. Luo, C. P.; Weatherly, G. C. The Invariant Line and Precipitation in a Ni 25 wt %Cr Alloy. *Acta Metall.* **1987**, *35*, 1963–1972.
17. Wayman, C. M. *Introduction to the Crystallography of Martensitic Transformations*; Macmillan: NY, 1964; pp 36.
18. Liu, H. W.; Yuan, Y.; Liu, Z. G.; Liu, J. M.; Zhao, X. N. Invariant Line Theory and the Crystallography of $L1_2$-$(Al, Ag)_3Ti$ Phase in Ag-modified $L1_0$-TiAl Based Intermetallic. *Scr. Mater.* **2006**, *54*, 1087–1092.
19. She, X. The Role of Ag-O-Al Species in Silver-Alumina Catalysts for the Selective Catalytic Reduction of NOx with Methane. *J. Catal.* **2006**, *237*, 79–93.
20. Penn, R. L.; Banfield, J. F. Imperfect Oriented Attachment: Dislocation Generation in Defect-free Nanocrystals. *Science* **1998**, *281*, 969–971.
21. *International Tables for X-ray Crystallography*, Springer: Dordrecht, The Netherlands, 2006; Vol. A, pp 78−85.
22. Thoelen, C.; Paul, J.; Vankelecom, I. F. J.; Jacobs, P. A. Spherical MCM-41 as Support Material in Enantioselective HPLC. *Tetrahedron: Asymmetry* **2000**, *11*, 4819–4823.
23. Lai, Z.; Bonilla, G.; Diaz, I.; Nery, J. G.; Sujaoti, K.; Amat, M. A.; Kokkoli, E.; Terasaki, O.; Thompson, R. W.; Tsapatsis, M. Microstructural Optimization of a Zeolite Membrane for Organic Vapour Separation. *Science* **2003**, *300*, 456–460.
24. Figuerola, A.; van Huis, M.; Zanella, M.; Genovese, A.; Marras, S.; Falqui, A.; Zandbergen, H. W.; Cingolani, R.; Manna, L. *Nano Lett.* **2010**, *10*, 3028–3036.